

Pulsed Terahertz Transmission Spectroscopy of Liquid CHCl₃, CCl₄, and their Mixtures

B. N. Flanders,[†] R. A. Cheville,[‡] D. Grischkowsky,[‡] and N. F. Scherer^{*,†}

Department of Chemistry, University of Pennsylvania, Philadelphia, Pennsylvania 19104-6323,
and School of Electrical and Computer Engineering and Center for Laser Research,
Oklahoma State University, Stillwater, Oklahoma 74078

Received: April 1, 1996; In Final Form: May 29, 1996[⊗]

The frequency-dependent absorption coefficient of CHCl₃, CCl₄, and their mixtures are measured by pulsed terahertz time domain transmission spectroscopy. The absorbance spectrum for neat CHCl₃ is shown to compare well with existing experimental data including coverage of the previously difficult to access 0.3–0.9 THz range. Furthermore, fitted curves to the absorbance spectra of the liquid mixtures, based on mole fraction weighted sums of the absorption coefficients of pure CHCl₃ and CCl₄, indicate the presence of a bulk dipole reducing mechanism, possibly due to clustering of CHCl₃ molecules about CCl₄. An algebraic extension of the mole fraction weighted fits allows discrimination between relative strengths of the various bimolecular absorption processes. The integrated absorption coefficient for collisionally induced absorption of CHCl₃–CCl₄ collisions was found to be less than that for CHCl₃–CHCl₃ collisions by 2.6 ± 0.4 THz cm⁻¹ (integrated absorption coefficient units). Finally, a new procedure for applying Mori's third-order continued fraction to a description of absorption line shapes in liquids is presented. Attempts to fit the observed absorption spectra to the line shape derived from the third-order truncation of Mori's continued fraction were unsuccessful. However, a constrained sum of Mori line shapes was found to fit the low and middle frequency portions of the spectrum reasonably well. This problematic behavior of the Mori analysis may not only exemplify nonexponential relaxation of the intermolecular torques, a known problem associated with the third-order truncation, but also the existence of two (or more) types of motion (i.e., translations, rotations, and possibly collective motions) causing relaxation of the dipolar correlation function. This improvement in the closeness of the Mori absorbance line shape fit to the experimentally determined data illustrates the possibility of straightforward extraction of dynamical properties of liquids from absorbance spectra. This theory provides an analytical, yet limited, alternative to the more complicated but more comprehensive determination of dynamical properties obtained through molecular dynamics simulations.

I. Introduction

The problem of describing the response of a dipole to absorption of electromagnetic radiation and the subsequent relaxation caused by fluctuations of the surrounding medium has been a central focus of condensed-phase studies for nearly the entire century.¹ One ongoing challenge is to understand the magnitudes and time scales of the several kinds of intermolecular interactions in polar, and therefore electrostatically associated, liquids.^{2,3} In principle, much of this information is obtainable through measurement and quantitative analysis of the far-infrared (FIR) absorption spectrum of the liquid in question.⁴

The far-IR absorbance data for liquids are also of relevance in the effort to elucidate the complicated dynamics that occur during the course of a chemical reaction,^{5,6} such as an inter- or intramolecular optically induced electron transfer in that solvent.^{7–9} Describing the role the solvent plays in the creation of a suitable minimum energy pathway from the reactant to the desired product¹⁰ (i.e., a nonequilibrium process) might be elucidated by the acquisition of a series of transient absorbance spectra of the solvent during the reaction. Experiments with a focus on the measurement of solvent properties (i.e., vibrational line shifts) in response to solute excitation have recently been published.¹¹ Terahertz (1 THz = 33.3 cm⁻¹ = 4.1 meV) studies, which directly probe the orientational and translational motions of the solvent, might provide additional insight into the details

of such solvent responses. A reasonable introduction to the problem of solvent response to chemical reaction is the determination of the processes and related time scales by which the solvent molecules fluctuate and relax in an equilibrium system, that is, in the absence of the strong perturbation produced by a reacting chromophore. Linear response theory and the fluctuation–dissipation theorem provide a starting point for using this equilibrium spectrum to model the solvent response to a chemical reaction. Hence, determining these solvent dynamics is directly related to knowing the solvent modes available for acceptance of excess energy (i.e., frequency-dependent friction) during the course of a reaction.^{4,12}

Dipolar absorption in the far-IR spectral range, 0–150 cm⁻¹, arises from orientational chromophore motions and collisional interactions of the molecular dipoles; the latter mechanism is also the cause of absorption for molecules with no permanent electric dipole moment. In the gas phase where intermolecular interactions are infrequent, the dipolar absorption spectrum displays a series of sharp lines centered at the rotational energy differences of the free molecule. The collisional broadening that occurs is well described by the van Vleck–Weisskopf line shape at low frequencies (<1 THz), by the Lorentzian line shape at high frequencies (>1 THz), and by a phenomenological switching function between them.¹³ In the simplest model for dipolar absorption in the liquid phase, formulated by Debye in 1912,¹ each free rotational absorption line is strongly collisionally broadened and the corresponding line shape is a Lorentzian. The Debye model predicts relaxation of the medium in the time required for randomization of the orientations of the dipoles.

[†] University of Pennsylvania.

[‡] Oklahoma State University.

[⊗] Abstract published in *Advance ACS Abstracts*, July 1, 1996.

Intermolecular collisions, which dissipate the energy absorbed from an applied field, bring about the decay of the initial, photoselected orientational distribution. This randomizing process is described by the molecular dipole–dipole correlation function $\langle \hat{u}(0)\hat{u}(t) \rangle$. This correlation function decays exponentially with a time constant of τ_D , a process termed Debye relaxation or rotational diffusion. An important assumption of the rotational diffusion model of dielectric relaxation is that only collisional interactions affect the absorption line shape; electrostatic intermolecular interactions are not considered in any way.¹ However, if correlations between the primary variable (in this case, the molecular dipole moment) and higher order terms in its Taylor series expansion (that is, the physical properties these terms describe, such as angular momentum and intermolecular torque) exist for times comparable to the time scale of rotational diffusion, then the relaxation of the dipolar correlation function will not be well described by the single exponential Debye time constant. An analytical theory that considers relaxation processes that decay on the same time scale as rotational diffusion is, therefore, of value.

The time domain terahertz transmission waveforms obtained in the present experiments are directly related to the molecular dipole correlation functions for the various mixtures. Linear response indicates that Fourier transformation of the measured dipolar correlation function leads to the corresponding dipolar absorption spectrum of the system. However, the measured function reflects all the dipole-modulating processes occurring in the liquid. In addition to simple rotational diffusion, a myriad of other processes are expected in these dipolar, and thereby electrostatically interacting, liquids.¹⁰ These include librational dissipation, viscous drag, and a range of phenomena concerning the response of the “reaction field” polarization of the surrounding solvent molecules to the reorientation of a dipole.^{14–18} Similarity in the decay times of these processes complicates the information that can be extracted from the absorption profile of the liquid.

The present experiments extend earlier pulsed terahertz transmission studies¹⁹ of nonpolar liquids to the polar regime. To our knowledge, only one other pulsed terahertz transmission study of polar liquids has been made,²⁰ although the experimentally challenging technique of reflection spectroscopy has been used to measure the temperature dependence of a portion of the far-IR spectrum of liquid water.²¹ The present measurements of the dipolar absorption spectra of the pure liquids CHCl₃ and CCl₄ and their mixtures are performed using a laser-gated Hertzian antenna source and receiver system developed by one of us.²² Briefly, the frequency-dependent absorbance of the nearly single-cycle terahertz pulse is recorded for different solutions. The gated detector directly measures the terahertz radiation field, thereby facilitating direct determination of the complex linear polarization, or susceptibility, of the sample. Fourier transformation allows the extraction of the frequency-dependent absorption coefficient by the approach described in Appendix A.

In this study, a qualitative explanation of the absorption coefficient spectra of the various mixtures is offered. Effort was made to separate the collisionally induced absorption (CIA) contribution from the observed spectra (see Appendix B). The relative absorption strength between heteromolecular and homomolecular collisions is reported. A second-order memory function analysis based on Mori’s continued fraction formalism is used to describe the absorbance spectra of the mixtures. This theory explicitly treats the rotational relaxation of molecules with nonzero moments of inertia. Since motion and fluctuations of the dipolar molecules are the dominant mechanism by which

radiation is absorbed, the Mori analysis is expected to fit the polar mixtures best. These fitted curves provide a series of decay times for the intermolecular torques, which are assumed to decay exponentially. Although application of the Mori formalism to the determination of dipole correlation functions in liquids is known to be problematic,¹⁶ the relative ease in using its closed form analytical results, compared to running molecular dynamics simulations, for example, provides incentive for exploring improved ways of applying the theory.

II. Theory

The Langevin equation, historically developed to describe the Brownian motion of a tagged particle moving in a condensed phase,^{23–25} is often used to describe the evolution of a dynamical variable, such as the dipole moment vector \hat{u} of a molecule in a liquid. Mori’s derivation²⁶ of the continued fraction representation of a generalized form of the Langevin equation, originally derived in 1960,²⁷ is presented in Appendix C. Since the original presentation of the continued fraction formalism²⁵ for expressing a correlation function was rather detailed, the theory section of this paper focuses the derivation to more clearly show how the memory functions are arrived at. This development of an expression for the molecular absorption coefficient follows directly from eq C16 in Appendix C.

The quantities $f_{j-1}(t)$ and $f_j(t)$ are molecular variables (related to the $(j-1)$ th and j th time derivatives of the primary variables as discussed below) whose finitely decaying time correlation functions are assumed to be responsible for the non-Markovian condition that the random force term of the Langevin equation is not delta-correlated. Instantaneous decay of the random force correlation function is required by the second fluctuation–dissipation theorem. The $f_j(t)$ term, defined for the specific case of $f_1(t)$ in eq C7b, is the component of the derivative of $f_{j-1}(t)$ that is perpendicular to the orientation of $f_{j-1}(0)$. Hence, $f_1(t)$ and $f_2(t)$ are variables directly related to the first and second time derivatives of the dipole moment vector $\mathbf{f}_0(t)$. In the current application, where the experimental observable is the sum of components of molecular dipole moments aligned with the polarization axis of the terahertz beam, $f_1(t)$ and $f_2(t)$ are closely related to the angular velocities and intermolecular torques, respectively, of the dipoles in the liquid.

The important result from Appendix C is the function $\Xi_j(t)$, the autocorrelation function of the j th component of the total force $\mathbf{f}(t)$. Laplace transformation of eq C16 leads to²⁵

$$\Xi_j(z) = \frac{1}{z - i\omega_j + \Xi_{j+1}(z)\Delta_{j+1}^2} \quad (1)$$

where

$$\Delta_j^2 = (f_j^* f_j)(f_{j-1}^* f_{j-1})^{-1} \quad (2)$$

and * means complex conjugate. Expansion of eq 1 for the case of $j=0$ yields an exact expression for the time correlation function of $\mathbf{f}_0(t)$, as described above. A truncation after the third-order expansion for $\Xi_0(z)$ gives

$$\Xi_0(z) = \frac{1}{z - i\omega_0 + \frac{\Delta_1^2}{z - i\omega_1 + \frac{\Delta_2^2}{z - i\omega_2 + \Delta_3^2 \Xi_3}}} \quad (3)$$

This result is the third-order Mori continued fraction. By assuming that the time derivative of $f_j(t)$ is uncorrelated with

$f_j(t)$, then $\omega_0 = \omega_1 = \omega_2 = 0$ (see eq C13b), and eq 3 can be simplified and rewritten as

$$\Xi_0(z) = \frac{z^2 + \Delta_3^2 \Xi_3(z)z + \Delta_2^2}{z^3 + \Delta_3^2 \Xi_3(z)z^2 + (\Delta_1^2 + \Delta_2^2)z + \Delta_1^2 \Delta_3^2 \Xi_3(z)} \quad (4)$$

Inverse Laplace–Fourier transformation of eq 4, given below in eq 10, results in an expression proportional to the absorption coefficient, $\alpha(\omega)$, the basis for the current data analysis.

By re-expressing some of the terms in eq 3, an equivalent expression in the memory function symbolism can be derived; this terminology better lends itself to comparison with other results in the literature.¹⁹ In particular, the second-order memory function, $K_2(z)$, may be substituted for the third expansion in eq 3, that is

$$K_2(z) = \frac{\Delta_2^2}{z + \Delta_3^2 \Xi_3} \quad (5)$$

Laplace transformation of eq 5 yields

$$K_2(t) = \Delta_2^2 e^{-(\Delta_3^2 \Xi_3)t} \quad (6)$$

Physically, this expression assumes that the intermolecular torque correlations decay exponentially, but mathematically originates in the truncation after the third expansion in eq 3. This truncation, which occurs in Laplace space, results in a Lorentzian function. Hence, transformation of this function back into time space results in an expression exponential in time, as shown in eq 6. The following associations can be made:

$$K_2(0) = \Delta_2^2 \quad (7)$$

and the damping constant for the orientational motion is

$$\gamma = \Delta_3^2 \Xi_3 \quad (8)$$

The first-order memory function, $K_1(z)$, is associated with the Laplace transformation of the autocorrelation function of f_1 , which is closely related to the angular momentum. This memory function is associated with the second expansion in eq 3. After transformation of $K_1(z)$ back into time space, $K_1(0)$ may be defined as

$$K_1(0) = \Delta_1^2 \quad (9)$$

Substitution of eqs 7–9 into the inverse Laplace transformation of eq 4 and Fourier transformation of the time domain function yields

$$\text{Re}[\Xi_0(i\omega)] = \frac{K_1 K_2 \gamma}{\gamma^2 (K_1 - \omega^2)^2 + \omega^2 [\omega^2 - (K_1 + K_2)]^2} \quad (10)$$

Multiplying eq 10 by the amplitude factor M ,

$$M = \frac{\epsilon_0 - \epsilon_\infty}{n(\omega)c} \quad (11)$$

and also by ω^2 yields the frequency-dependent absorption coefficient

$$\alpha(\omega) = M\omega^2 \text{Re}[\Xi_0(i\omega)] \quad (12)$$

which is the main result of this application of Mori theory. This absorption coefficient is compared with the experimental $\alpha(\omega)$ determined as described in Appendix A.

Analytical expressions for K_1 , K_2 , and γ have been determined for solvents of various molecular symmetries.^{16,28} For the case of chloroform, a symmetric top, K_1 is

$$K_1 = \frac{2k_B T}{I_B} \quad (13a)$$

However, eq 13 is the square of the mean free rotational frequency. Since the experimental observable is the sum of the projections of the molecular dipole moments onto the polarization axis of the terahertz beam, eq 13 must be corrected to account for the collective nature of the observed rotational motion. For motions of molecules transverse to the polarization axis, the appropriate parameter is¹⁶

$$K_1^{xx} = K_1 \frac{2\epsilon_0 + 1}{3\epsilon_0} \quad (13b)$$

where ϵ_0 is the zero frequency dielectric constant. For motions of the molecules longitudinal to the polarization axis the appropriate parameter is¹⁶

$$K_1^{zz} = K_1 \frac{2\epsilon_0 + 1}{3} \quad (13c)$$

The appropriate expression for relating K_2 and γ may be expressed as¹⁶

$$\gamma = \frac{\epsilon_0 g^S}{K_1} \left(\frac{3}{2\epsilon_0 + \epsilon_{00}} \right) \frac{K_2}{\tau_D} \quad (14)$$

where either K_2 or γ is treated as an adjustable parameter. In eq 13 the moment of inertia $I_B = 2.54 \times 10^{-45}$ kg/m², and $T = 298$ K. The corresponding values are used in eq 14 in addition to $\epsilon_0 = 4.71$,^{16, 29} $\epsilon_\infty = 2.13$, the Kirkwood constant $g^S = 1$, and $\tau_D = 6.36$ ps.¹⁶

III. Experimental Section

A. Apparatus. Pulses of less than 100 fs are generated in a Kerr lens mode-locked Ti:sapphire oscillator of standard design.^{30–32} The output of the laser (90 MHz pulse train, 300 mW average power) was split into pump and probe beams sent through scanning and fixed delay lines, respectively, and focused with doublet lenses ($f = 2.5$ cm) onto the semiconductor source and receiver chips.

Figure 1a illustrates the terahertz time domain spectroscopy setup (see refs 13, 22, and 34 for more details). The transmitting antenna structure of Figure 1b is composed of two 10 μm wide gold transmission lines on a gallium arsenide wafer. The separation between the parallel lines is 80 μm . The “H”-shaped receiving antenna, shown in Figure 1b, is a 20 μm long gold structure fabricated on silicon-on-sapphire substrates. Transmission lines 5 μm wide, 1 μm thick, and 20 mm long connect the antenna to contact pads. An 80 V bias is applied to the transmitter. The 780 nm light serves to produce a sudden population of carriers in the region of the GaAs very close (within 5 μm) to the anode and in the 5 μm gap in the receiver. The carriers are accelerated by the applied bias and incident terahertz field in the source and receiver, respectively; the pulsed terahertz fields are thereby emitted and detected. The terahertz radiation was collected by a high-resistivity Si lens and collimated and directed by paraboloidal optics onto the receiver antenna. The incoming electrical pulse was detected by optically gating the receiver and measuring the current flow driven by the instantaneous voltage of the terahertz electric field. A

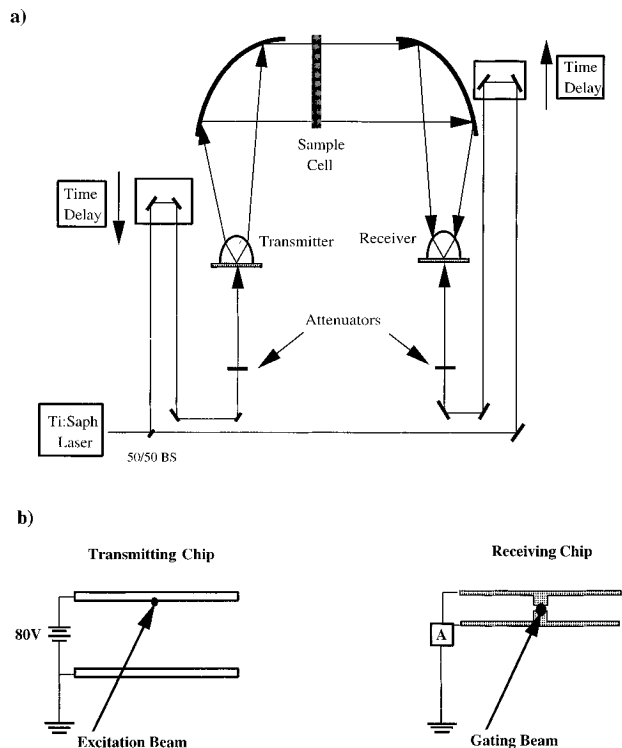


Figure 1. (a) Terahertz time-gated spectrometer. Upon excitation by the optical pump pulse (approximately 50 fs), the transmitting (source) chip emits the terahertz pulse, which is directed through the sample cell with a 2 mm path length and 1 mm Si windows. Si lenses and Al paraboloids are used to direct the terahertz pulse through the cell and onto the back of the receiving chip. (b) Expanded view of the antenna structures on the source and receiving chips. The antenna on the receiver is the vertical section with a gap (5 μm) positioned at its center. The vertical section is 20 μm long, and the pair of horizontal lines that connect to the top and bottom of the antenna are 5 μm wide.

precision stepper motor delay line (Melles Griot, Nanomover) was used to vary the path length of the optical beam illuminating the source and thereby scan the temporal profile of the terahertz pulse at the receiver. The pump beam intensity is modulated with a mechanical chopper at 2 kHz, and the current induced in the receiver is amplified (Centronic PA-100 or Stanford Research Systems SR570) by a gain factor of 10^8 V/A and processed in a digital lock-in amplifier (Stanford SRS-830) referenced to the chopper. Figure 2 shows the terahertz pulse and corresponding frequency spectrum. This combination of chip design and material has a frequency response extending out to roughly 4 THz. The second waveform (points and dashed line) in Figure 2b is obtained using another source: a 30 μm long antenna on an SOS chip, similar to the receiver discussed above. This earlier version terahertz spectrometer gave the same absorption spectra shown below, but the useful spectral range was only about 2 vs 4 THz for the GaAs source.

The sample cell, composed of a machined stainless steel ring (2.0 mm or 10.0 mm thick, 6.0 cm inner diameter) sandwiched between two 1 mm Si windows, was inserted between the two paraboloids, thereby allowing interrogation with a collimated beam of terahertz radiation (0.1–4.0 THz, 0–133.3 cm^{-1}). Essentially identical results were obtained using high-density polyethylene (HDPE) windows, except that the HDPE absorbs frequencies above 2 THz, so the measured absorbance data were limited to a rather narrow spectral range (0–2.0 THz). High-resistivity Si windows, however, exhibited significantly more surface reflection loss than HDPE owing to their larger index of refraction. All mixtures were measured in the 2.0 mm path length cell except for neat CCl₄, which, due to its low absorption

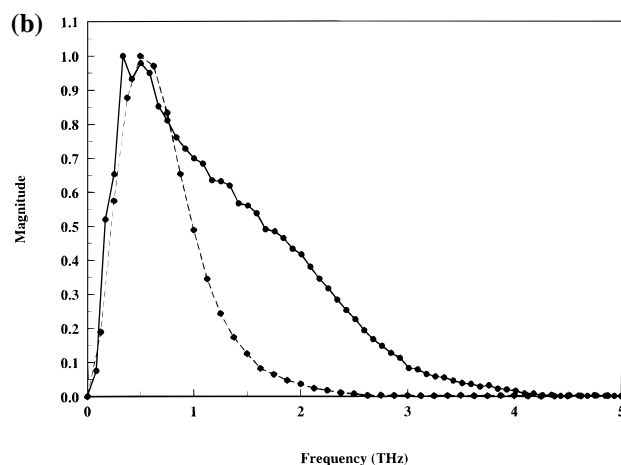
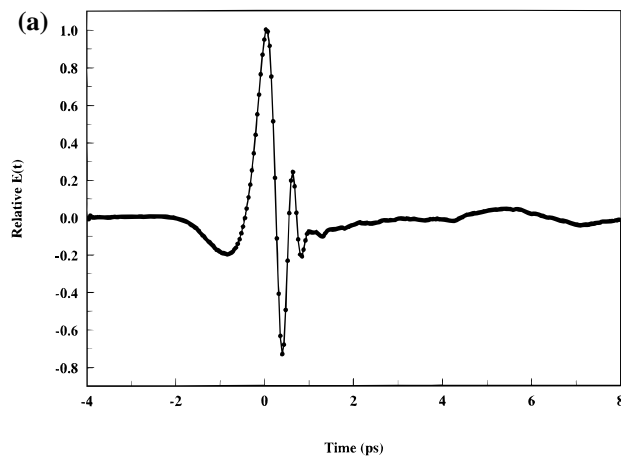


Figure 2. (a) Measured terahertz pulse and (b) amplitude spectrum of measured terahertz pulse compared to terahertz pulse of 30 μm antenna source on an SOS chip.

coefficient, was measured in a 10.0 mm path length cell. Each spectrum is the result of two sets of five 300 data point scans, each requiring 6 min for acquisition, except that of neat CCl₄, which was composed of two sets of five 325 data point scans.

Results and Discussion

A. Temporal Waveforms. Figure 3a shows the terahertz pulse temporal waveforms that result from transmission through the samples. The time domain data sets were shifted relative to one another such that the maximum of the transmitted waveform occurred at the same time delay. This point was assigned to be the zero of time. The NMR or FTIR technique of zero padding³³ was not used in the transforming of the data from the time to the frequency domains, since the frequency domain signals were of sufficient resolution. The terahertz signal does not, however, recover fully to zero in the 8 ps following the pulse peak giving rise to an increase in the amplitude of the lowest frequency data point in some of the frequency spectra. Longer scans would eradicate this problem, but reflections off the substrate interfaces in the source chip contaminate the data beyond 8 ps. Hence, scans are truncated roughly 8 ps after the trailing edge of the pulse.

B. Extraction of $\alpha(\omega)$. Two separate measurements are required for a complete data set: (1) the terahertz transmission spectrum through the empty cell and (2) the terahertz spectrum through the cell plus liquid sample for each of the six different samples. The determination of the absorption coefficient from the experimental time domain data is similar to that of Katzenellenbogen et al.³⁴ (also see Harde et al.³⁵) and is

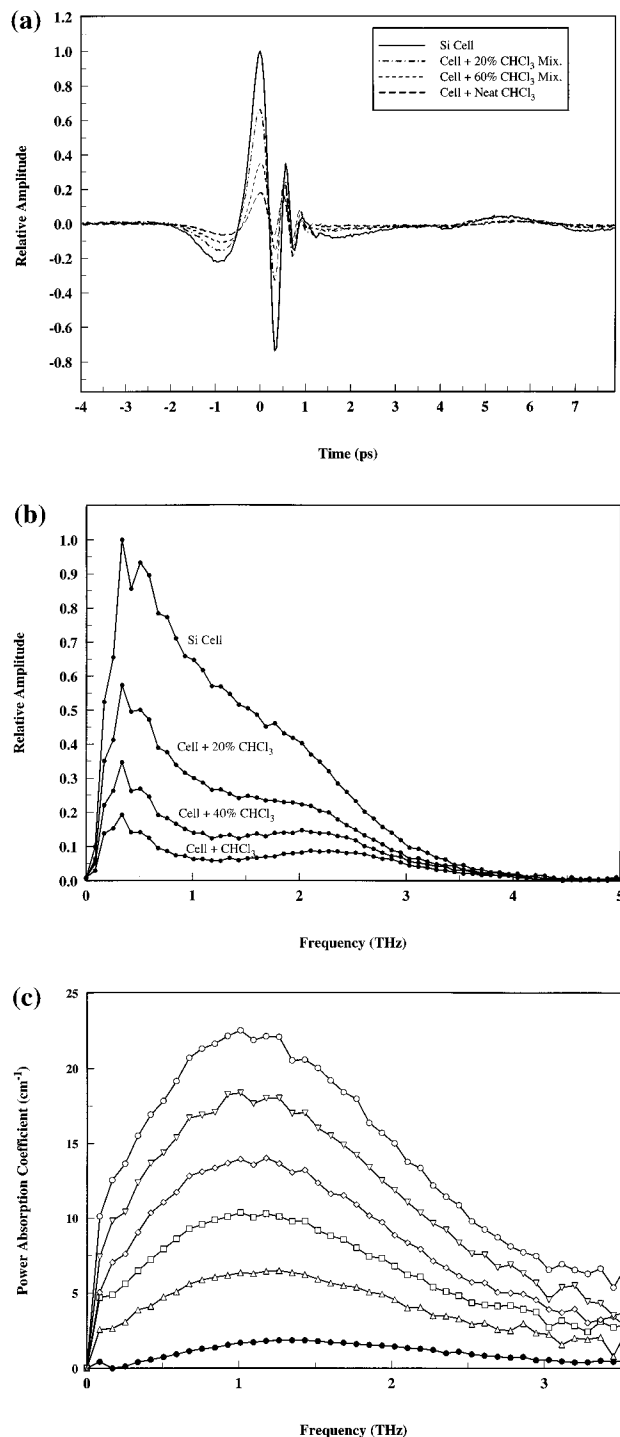


Figure 3. (a) Measured terahertz pulses transmitted through the empty cell, the 20% and 60% mixtures, and neat CHCl₃. (b) Frequency domain amplitude spectra of the transmitted pulses for the same samples. (c) Frequency-dependent absorption coefficient of each of the series of solutions of CHCl₃ and CCl₄. Boldface circles denote pure CCl₄, triangles denote 20% (by volume) CHCl₃, squares denote 40% CHCl₃, diamonds denote 60% CHCl₃, inverted triangles denote 80% CHCl₃, and circles denote pure CHCl₃.

reviewed in Appendix A. The magnitude spectra and frequency-dependent absorption coefficients for all the solutions are shown in parts b and c of Figure 3.

C. Quality of CHCl₃ Data. Figure 4 gives a comparison of the terahertz data for the frequency-dependent absorption coefficient of CHCl₃ to the FTIR data of Goulan et al.³⁶ The reliability of the current technique is demonstrated by the good agreement between the data sets below 0.15 THz and above 0.75 THz. A more recently assembled microwave-FIR spec-

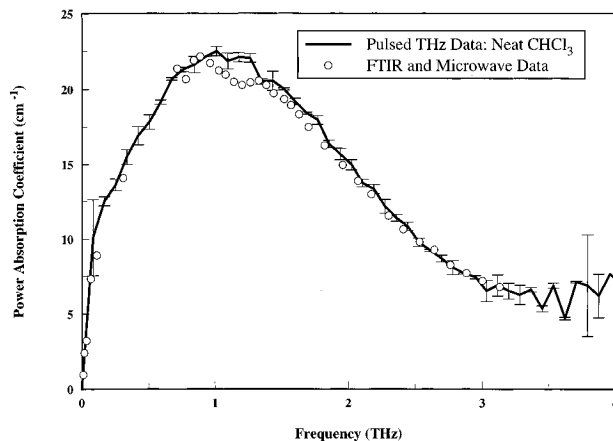


Figure 4. Comparison of the present measured absorption coefficient (solid points) with earlier data measured by Goulan et al. using microwave and FTIR techniques³⁶ (open points). These conventional techniques only sparsely probe the 0.3 and 0.9 THz range, whereas pulsed terahertz spectroscopy readily accesses this region.

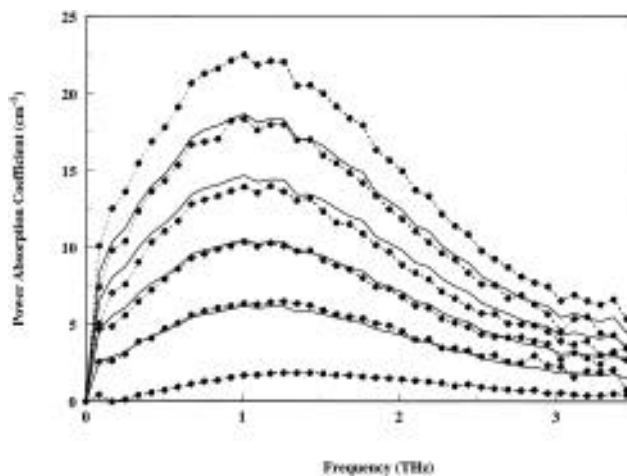


Figure 5. Mole fraction weighted Beer's law fits to the absorption coefficient for each of the series of mixtures. The dashed curves and boldface circles denote the experimental data, while the solid curves denote the fits.

trum³⁷ of CHCl₃ matches the terahertz data with equal precision. The ability of the terahertz pulse to probe the sample in the 0.3–1.0 THz range is especially useful. This portion of the spectral response is particularly difficult to establish because neither microwave nor FTIR techniques allow continuous spectral measurements across this region.³⁷ Figure 2b indicates that the terahertz pulses employed here have their maximum spectral amplitude at roughly 0.5 THz and, therefore, are quite intense across this region. The error bars shown reflect the standard deviation between separate measurements. Hence, they also reflect the absolute reproducibility over a several day period between measurements.

D. Mole Fraction Weighted Fitting. Figure 5 illustrates the use of the mole fraction weighted expression as a function of the absorption coefficients for the pure liquid components, given by eq B1 in Appendix B, to calculate the absorption coefficient data for the mixtures of CHCl₃ and CCl₄. The quality of the fits is poorest for the more polar mixtures (i.e., those with the greatest concentration of CHCl₃) but improves as the concentration of CHCl₃ decreases. This trend may suggest that for a particular mixture, reduction of the bulk dipole moment occurs through intermolecular interactions and that the magnitude of this reduction in absorption strength is greatest in mixtures less concentrated in CHCl₃ molecules. A possible

explanation is that some clustering of chloroform about the nonpolar carbon tetrachloride is occurring. The grouping of dipoles about the nonpolar component might cause some degree of cancellation between the individual molecules' dipolar fields and, thereby, reduction of the bulk dipole moment. As the concentration of CHCl₃ decreases across the series, the degree of "clustering" is expected to fall off because the number of polar molecules available for grouping around a single nonpolar molecule (and consequential cancellation of individual dipolar fields) is decreasing. Presumably in the least polar mixture, the number of CHCl₃ molecules is simply too small to allow this cancellation effect to occur within the precision of the data. Calculations of the radial distribution functions (from molecular dynamics simulations) for each of the mixtures that should clarify whether the clustering effect is actually occurring are currently underway.³⁸

The assumptions implicit in eq B1 are expected to have minimal effect on the trend evident in Figure 5. The improper weighting of α_{CHCl_3} overestimates the absorbance contribution of CHCl₃ because both permanent dipolar absorption (PDA) and collisionally induced absorption (CIA) components of α_{CHCl_3} in eq B2 are weighed linearly in x_{CHCl_3} rather than linearly for α_A (the PDA term) and quadratically for α_{AA} (the CIA term). For example, suppose that the four mixtures have mole fractions of CHCl₃ of 0.2, 0.4, 0.6, and 0.8. (The reader should note that these are not the mole fractions of the mixtures used in this experiment but rather hypothetical values merely introduced here to illustrate a point. They were chosen because they are simpler to rapidly compute than the actual mole fractions given in the table. Of course, all analysis of the experimental data used the actual values and not the hypothetical values given here.) If the $\alpha_{\text{CHCl}_3-\text{CHCl}_3}$ contribution were weighted linearly in x_{CHCl_3} (which, by substitution of eq B2 into eq B1, is the present case) rather than quadratically, α_{mix} for each of the four mixtures would be artificially large by an additive term (found by simply computing the difference $x_{\text{CHCl}_3}\alpha_{\text{CHCl}_3-\text{CHCl}_3} - x_{\text{CHCl}_3}^2\alpha_{\text{CHCl}_3-\text{CHCl}_3}$) of $0.16\alpha_{\text{CHCl}_3-\text{CHCl}_3}$, $0.24\alpha_{\text{CHCl}_3-\text{CHCl}_3}$, $0.24\alpha_{\text{CHCl}_3-\text{CHCl}_3}$, and $0.16\alpha_{\text{CHCl}_3-\text{CHCl}_3}$, respectively. However, The second assumption invoked in the use of eq B1, the neglect of CIA between CHCl₃ and CCl₄ molecules, artificially decreases the predicted absorption coefficient for the mixture. For example, for a (again, hypothetical) series of mixtures corresponding to $x_{\text{CHCl}_3} = 0.2, 0.4, 0.6,$ and 0.8 , neglect of the heteromolecular CIA term (as is done in eq B1), properly expressed as $x_{\text{CHCl}_3}(1 - x_{\text{CHCl}_3})\alpha_{\text{CHCl}_3-\text{CCl}_4}$, would yield α_{mix} values that would be artificially small by an additive term of $0.16\alpha_{\text{CHCl}_3-\text{CCl}_4}$, $0.24\alpha_{\text{CHCl}_3-\text{CCl}_4}$, $0.24\alpha_{\text{CHCl}_3-\text{CCl}_4}$, and $0.16\alpha_{\text{CHCl}_3-\text{CCl}_4}$, respectively. Therefore, in the case for $\alpha_{\text{CHCl}_3-\text{CHCl}_3} = \alpha_{\text{CHCl}_3-\text{CCl}_4}$, the two assumptions implicit in eq B1, the overweighting of the $\alpha_{\text{CHCl}_3-\text{CHCl}_3}$ and the neglect of the $\alpha_{\text{CHCl}_3-\text{CCl}_4}$ contributions, exactly cancel!

The computation in eq 15 below indicates that equating $\alpha_{\text{CHCl}_3-\text{CHCl}_3}$ to $\alpha_{\text{CHCl}_3-\text{CCl}_4}$ does not appear to be a good assumption; the surprisingly large difference of -2.6 THz cm^{-1} between α_{AB} and α_{AA} indicates that of the two assumptions, that associated with α_{AA} should cause the greatest error in the fitted curves. Even so, effects due to the evidently large magnitude of α_{AB} and the corresponding assumption of improper weighting of CIA between CHCl₃ molecules are not apparent in the data in Figure 5. That is, the large magnitude of $\alpha_{\text{CHCl}_3-\text{CHCl}_3}$ relative to $\alpha_{\text{CCl}_4-\text{CHCl}_3}$ indicates that the first assumption (discussed above) is the dominant one of the two oversights implicit in eq B1. As follows from the foregoing discussion, if the overweighting of $\alpha_{\text{CHCl}_3-\text{CHCl}_3}$ contributed significantly to the fits to the spectra, then the overestimation

of the fits to the data would be greatest for the mixtures closest to being equal in CCl₄ and CHCl₃ concentration. As indicated above, the assumption is most severe when $x_{\text{CHCl}_3} = 0.5$. (Notice that the deviations for solutions of mole fraction 0.443 and 0.642 disagree with this conclusion.) However, the dominant trend displayed in Figure 5 is that of increasing overestimation of the experimental data by the Beer's law based fit with increasing x_{CHCl_3} . Therefore, the contribution of improper weighting of $\alpha_{\text{CHCl}_3-\text{CHCl}_3}$ is believed to be negligible.

E. Heteromolecular and Homomolecular CIA. Values for the difference between the integrated CIA coefficients for collisions between like and unlike molecules in mixtures of CHCl₃ (molecule type A) and CCl₄ (molecule type B) are calculated from the two quietest data sets according to the method described in Appendix B. The integrated differences between $\alpha(\omega)$'s (illustrated in Appendix B) for the 20% and 40% by volume of CHCl₃ solutions were averaged to give

$$\overline{\alpha_{\text{AB}} - \alpha_{\text{AA}}} = -2.6 \pm 0.4 \text{ THz} \cdot \text{cm}^{-1} \quad (15)$$

A comparison between the difference in eq 15 and pure CCl₄'s integrated absorption coefficient (also determined via a Simpson's rule integration technique) of $2.3 \pm 0.4 \text{ THz cm}^{-1}$ indicates that CIA between CHCl₃ molecules is at least roughly equal to the integrated CIA of CCl₄. Furthermore, because the magnitude of α_{AA} is significantly larger than that of α_{AB} , exact cancellation between the additive terms associated with the two assumptions implicit in eq B1 does not occur. This issue was discussed in greater detail in subsection D.

F. Mori Analysis. The absorbance spectra for CCl₄, CHCl₃, and their mixtures were fit to the absorption coefficient derived from the third-order truncation of Mori's general continued fraction formalism. The need for greater than first-order continued fractions indicates that Debye relaxation fails to completely describe the far-IR data because the time scale during which the correlation function for the molecular dipole moment decays is not sufficiently longer than the decay times of correlation functions of other molecular variables (i.e., the memory function in the generalized Langevin equation is not δ -function correlated). The third-order truncation of Mori's formalism assumes that the polar liquid relaxes not only by rotational diffusion but also through dielectric friction effects. This combination of relaxation mechanisms that contribute to the far-IR data complicates the determination of an analytical formula for the frequency-dependent absorption coefficient.

The application of a Mori function analysis to the data is most physically meaningful for neat polar liquids like CHCl₃ for which the absorption spectrum is dominated by the dipolar absorption of the permanent moment on chloroform. Parts a and b of Figure 6 show the fit of eq 12 to the neat CHCl₃ and CCl₄ data, respectively. The fitted curves represented by the solid lines use the four parameters M , K_1 , K_2 , and γ in an unconstrained way. The fit to CCl₄ is quite good, since the R^2 factor of the fit is 0.99, and the fit parameters are nearly identical with those reported by Keiding and co-workers.¹⁹ The unconstrained fit to CHCl₃ (dashed line, Figure 6a) is good but slightly less satisfactory, as the R^2 factor of 0.96 indicates. Furthermore, if the constraints on the parameters M , K_1 , and K_2 (eqs 11, 13, and 14) are invoked, the resulting fit to the data (either the dotted or dashed line in Figure 7, depending on choice of γ) is even worse. This constrained Mori expression was exhaustively adjusted in order to obtain higher quality fits, but strong disagreement with the data was apparent in all forms. These latter results suggest that a single Mori function is not appropriate for chloroform.

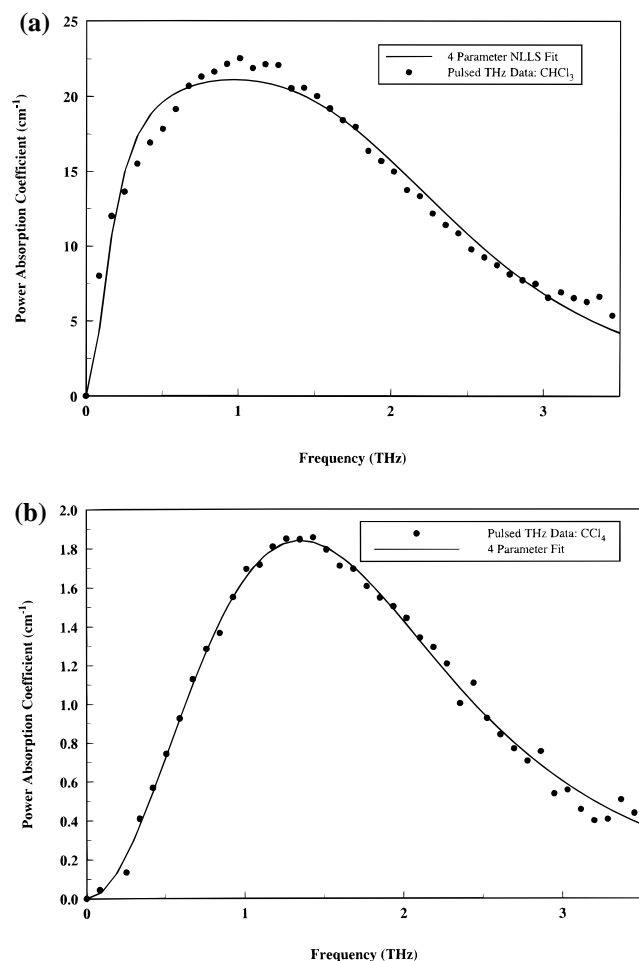


Figure 6. (a) Unconstrained nonlinear least squares (NLLS) four-parameter fit (solid line) to pure CHCl₃ data (points). The fit parameters are $M = 19.40$ ps/m, $K_1 = 11.33$ ps⁻², $K_2 = 239.16$ ps⁻², and $\gamma = 21.66$ ps⁻¹. (b) Unconstrained NLLS four-parameter fit to pure CCl₄ data. The fit parameters are $M = 0.40$ ps/m, $K_1 = 42.31$ ps⁻², $K_2 = 269.67$ ps⁻², and $\gamma = 27.10$ ps⁻¹.

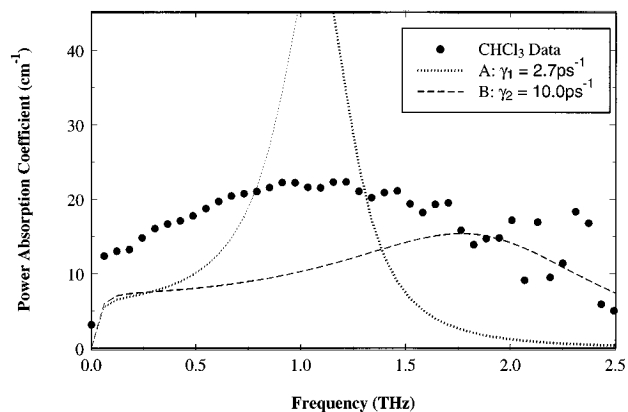


Figure 7. Neat CHCl₃ spectra and single Mori fits. Curves A and B are Mori line shapes derived with only one adjustable parameter apiece, and the solid curve through the hollow circles is the experimental data for neat CHCl₃. Parameters for curve A are $E = 39.6$ ps/m, $K_1 = 3.16$ ps⁻², $K_2 = 46$ ps⁻², and $\gamma = 2.7$ ps⁻¹, and the parameters for curve B are $E = 39.6$ ps/m, $K_1 = 3.16$ ps⁻², $K_2 = 170$ ps⁻², and $\gamma = 10$ ps⁻¹.

The good agreement to the carbon tetrachloride data in Figure 6b is, by contrast, surprising. The parameters cannot, in this case, be easily related to physical parameters such as molecular orientational motion of torques. (This spherical top molecule can only absorb terahertz radiation by the CIA mechanism.) Because CCl₄ is nonpolar, the absorption it undergoes is associated with the projection of a transient (collisionally

TABLE 1: Parameters for Bi-Mori Analysis

%vol	x_{CHCl_3}	M ps/m	K_1 (ps ⁻²)	K_1^{xx} (ps ⁻²)	K_1^{zz} (ps ⁻²)	$K_{2,A}$ (ps ⁻²)	$K_{2,B}$ (ps ⁻²)	γ_A (ps ⁻¹)	γ_B (ps ⁻¹)
100	1.000	42.12	3.24	2.39	11.25	210.0	104.0	12.50	12.50
80	0.827								
60	0.642								
40	0.443								
20	0.230								
0	0.000	0.60	27.4			200.0		10.00	

induced) dipole moment along the axis of the polarization of the terahertz beam. Therefore, K_1 and K_2 in eqs 13 and 14 are related to averages over the transient dipole moments the molecule obtains through intermolecular interactions.¹⁹ It is not clear that K_1 is related to the moment of inertia as eq 13 indicates, since the dipole moment responsible for CIA is not constrained to lie along any single molecular axis. For this reason, K_1 was unconstrained. The values for K_2 and γ listed in Table 1 are not related by eq 14 or by the analogous equation for a spherical top. In other words, the fit presented in Figure 6b uses three independently adjustable parameters. Only the leading amplitude factor M is calculated in a physically meaningful way, that is, according to eq 11. Therefore, the numbers chosen for K_1 , K_2 , and γ (see Table 1) to yield the best fit of the experimental data are viewed only as qualitative guidelines regarding the strengths of the various intermolecular forces that affect the dipole moment of the absorber.

G. Bi-Mori Analysis. A test of the veracity of the Mori function description of polar liquids would require that M and K_1 be determined independently. Application of eq 14 then further reduces the number of adjustable parameters to one. A best fit of the resulting form to the experimental data for CHCl₃ is obtained by varying γ . As illustrated by Kivelson and Madden,¹⁶ the result shown in Figure 6a and curves A and B in Figure 7, the single third-order Mori function is unable to fit the entire observed absorption band. Implicit in the third-order truncation is the assumption that the correlation function related to intermolecular torques, i.e., $\langle f_2(t)f_2(0) \rangle$, decays exponentially. It is not obvious that an exponential function provides the best description of this decay. Moreover, Kivelson et al.¹⁶ persuasively argue the invalidity of this assumption and conclude that a very probable reason for the poor fit is that the assumed exponential decay of the intermolecular torques is not correct. The development of the third-order Mori line shape is exact except for the assumed frequency independence of γ , or equivalently the exponential decay of $K_2(t)$, that is implicit in the truncation of eq 3. Therefore, any failure of the Mori line shape to reflect the observed line shape of the measured absorbance spectrum has been attributed to improper treatment of the torque relaxation, the physical process characterized by γ and K_2 .¹⁶

The fundamental idea of the Mori formalism is the explicit consideration of the dependence of the relaxation of the variable under observation (in this case, the bulk dipole moment along the polarization axis of the terahertz beam) on the relaxation of other slowly changing variables. In the third-order theory, these other variables are closely related to the angular momentum and the intermolecular torques. Any more rapidly oscillating variable, such as the rate of change of the intermolecular torques, is assumed to have become uncorrelated instantaneously on the time scale of the dipole moment relaxation. This condition should be met when the exponential decay constant for the intermolecular torques is large. Under the condition of $\gamma \gg \omega$, the torque correlation and that of all faster variables may well be essentially instantaneous on the time scale of the relaxation of the processes that characterize the low-frequency spectral region where ω is small. In this frequency region, the nature

of the torque decay might not be relevant. As long as the correlation relaxes very rapidly, the exponential description may be adequate because the relatively slow process of dipole relaxation corresponds to low-frequency components well separated from the large value of γ . Therefore, Mori absorption coefficient line shapes that are characterized by fast torque relaxation times might be expected to fit the low-frequency portion of the far-IR spectrum with reasonable success.

The absorption profile in the far-IR spectral region may be complicated by a cause other than a complicated decay of intermolecular torque. For instance, the existence of two types of motion and associated relaxation that can give rise to dipolar absorption could explain the need for a bi-Mori analysis. The idea that multiple absorption mechanisms contribute to dipolar absorption in the far-IR spectral region of liquids is consistent with the instantaneous normal mode analysis of polar liquid motions; rotational and translational modes have broad and overlapping spectral distributions.¹⁰ Moreover, no single type of molecular motion is believed to compose the entire 0–130 cm⁻¹ spectral band of liquids. Therefore, attempting to use only one Mori function to describe the low-frequency band might be expected to be problematic. That is, the Mori formalism characterizes the low-frequency spectrum with the parameters given in eqs 11, 13, and 14. Hence, the idea beneath the attempt to fit a single, properly constrained Mori line shape to observed data is that the spectral band is characterized by a single parameter, the torque relaxation time, for example. However, as different kinds of molecular motions are expected to exist in liquids, more than one Mori line shape may be required to construct an accurate fit to the experimentally determined absorption spectrum. Therefore, more than one set of Mori parameters (i.e., K_1 , K_2 , γ) may be chosen for each type of molecular motion. It is to this end that data analysis based on a sum of Mori line shapes was attempted.

Figure 8 illustrates the fitted curve of a “bi-Mori” line shape to the data for neat CHCl₃ as well as the two single Mori curves, denoted A and B, composing the fit. The fit was constructed in the following way. Equation 12 was used as the basic form of the Mori line shape for each component of the two-curve fit. The amplitude factor M , however, was effectively constrained. That is, the curves were scaled by factors of $A = 0.76$ and $(1 - A) = 0.24$, respectively. This constraint is imposed because M is proportional to the difference between the zero and infinite frequency dielectric constants and M is taken to represent the total absorption capability of the liquid. Therefore, the magnitude of each of the two Mori components was constrained. Curve A was fit with the parameters listed in the Table 1. Equation 13b for the collective parameter K_1^{xx} was used in computing curve A. This parameter is essentially the $t = 0$ value of the angular momentum correlation function. Equation 13c for K_1^{zz} was used in computing curve B. Furthermore, two parameters associated with the expression for the intermolecular torque relaxation rate in eq 14 are used: τ_D (in curve A) which is the Debye relaxation time describing rotational diffusion, and τ_L (in curve B) which is the longitudinal relaxation time. This value, expressed as³⁹

$$\tau_L = \frac{2\epsilon_\infty + 1}{2\epsilon_0 + 1} \tau_D \quad (16)$$

is smaller than the Debye relaxation time $\tau_D = 6.36$ ps, while $\tau_L = 3.13$ ps. The smaller value of τ_L relative to τ_D indicates a process faster than the occurrence of rotational diffusion. A candidate for this rapid behavior is a process of concerted or collective motion involving several molecules. The FIR absorp-

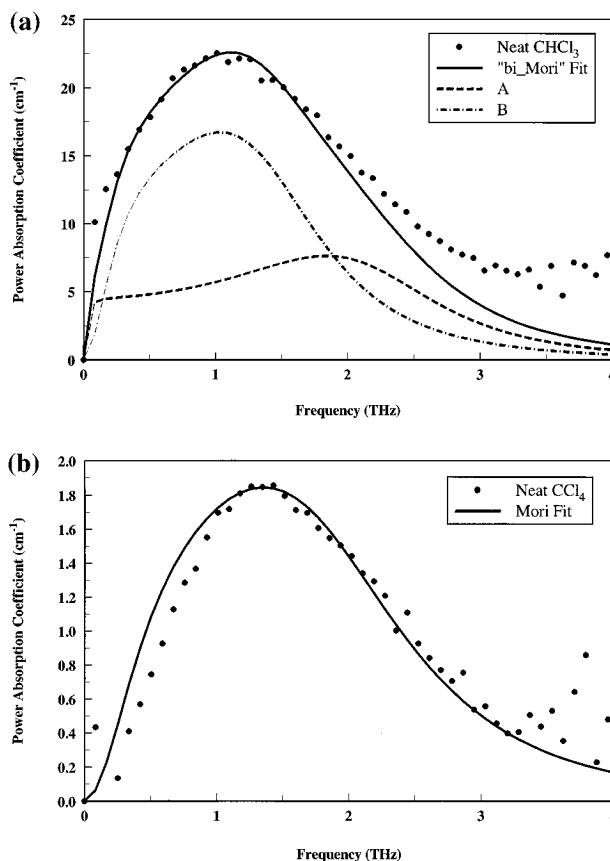


Figure 8. (a) “Bi-Mori” fit (solid line) to experimental data (solid points) for neat CHCl₃. Dashed lines represent the Mori line shapes, which compose the bi-Mori line shape. Fit parameters are listed in the Table 1. (b) Single Mori line shape (obtained by treating K_1 , K_2 , and γ as adjustable parameters) for neat CCl₄.

tion spectrum may be viewed as being composed of a diffusive contribution (curve A) and an inertial contribution (curve B). A constrained sum of Mori line shapes, the sums of curves A and B, was fit to the experimental data for CHCl₃ (see Figure 8a, solid line). This function for the constrained “bi-Mori” fit may be written as

$$\alpha_{\text{fit}}(\nu) = A\alpha_A(\nu) + (1 - A)\alpha_B(\nu) \quad (17)$$

where α_A and α_B are given by eq 12 with the changes made above and the three adjustable parameters are A , γ_A and γ_B . As a further constraint, $\gamma_A = \gamma_B$. A smaller number of fitting variables would be desirable, but in comparison to the four-parameter NLLS fits shown in parts a and b of Figure 6 (for neat CHCl₃ and CCl₄, respectively), the parameters used in the “bi-Mori” routine are chosen for physical reasons.

It is evident in Figure 8 that the constrained “bi-Mori” function fits the terahertz data much more closely than the constrained single Mori function. The closeness of the fit in the low-frequency region (0–2 THz) is especially good, and only above roughly 2 THz does the fit diverge from the data. This characteristic is consistent with the expectation (discussed above) that the Mori line shape should fit the low-frequency portion best. γ_A and γ_B were determined by the fits to be 12.5 THz (see Table 1). Therefore, the condition for appropriate application of the theory, that γ is much greater than the frequencies where the spectra is best fit, is borne out. The data are well fit at frequencies less than 15% of the torque relaxation rate.

Bi-Mori fits for each of the CHCl₃–CCl₄ mixtures are presented in Figure 9, and all the memory function parameters

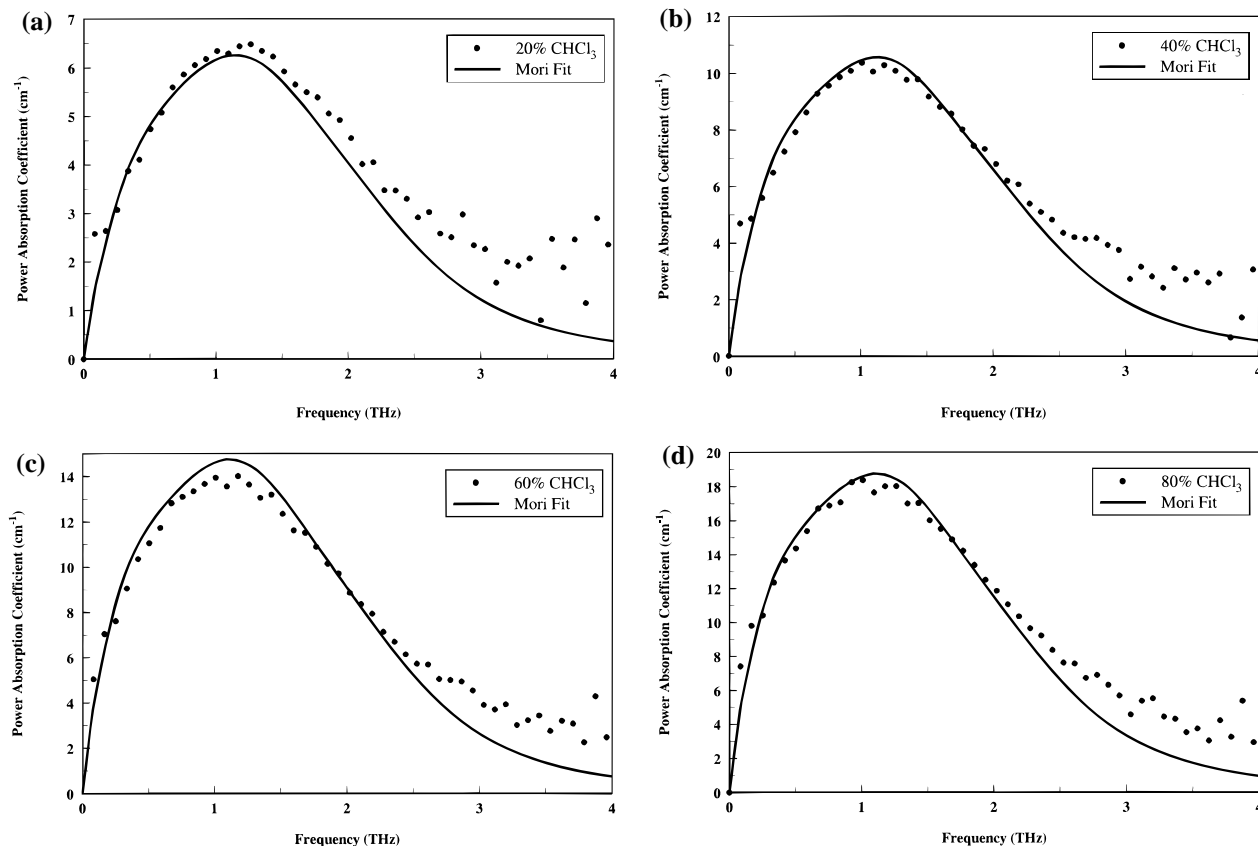


Figure 9. (a)–(d) Bi-Mori fits to the frequency-dependent absorption coefficients for the 20%, 40%, 60%, and 80% by volume CHCl_3 mixtures. The fitted curves were obtained by a mole fraction weighted sum of fits (shown in Figure 8) to the neat CHCl_3 and CCl_4 data.

are summarized in the table. These data are fit by a mole fraction weighted sum of the “bi-Mori” absorption coefficients for the neat liquids and closely fit the 0–2 THz spectral regime. However, the difficulty in applying the Mori theory to CCl_4 prevents elucidation of the possible changing nature of far-IR absorption across increasingly more polar solution series.

V. Conclusions

Computation of the difference in integrated magnitudes between $\alpha_{\text{CCl}_4-\text{CHCl}_3}$ and $\alpha_{\text{CHCl}_3-\text{CHCl}_3}$ has been used to verify the assumptions implicit in a fitting model, based on Beer’s law, that has been applied to the measured absorption coefficient spectra. These fits revealed reduced absorption strength of the data, compared to the fits, in mixtures more concentrated in CHCl_3 . This observation might indicate a partial cancellation of the expected bulk dipole moment (and, thereby, absorption strength) through clustering of CHCl_3 molecules about individual CCl_4 molecules.

A fitting routine based on the Mori line shape formalism has been presented and shown to yield quantitatively correct fits to experimental absorption coefficient data at low and intermediate frequencies (0–2 THz). The expectation that the model should succeed at low frequencies and begin to fail at frequencies comparable to the parameter representing the torque relaxation rate is borne out in the observation that the agreement between the model and the measured spectra decreases quickly above 2 THz, a value that corresponds to roughly 15% of the torque decay rate. The bi-Mori analysis convincingly characterizes the contributions of two molecular processes to the far-IR spectrum. These two processes are determined to compose 76% and 24% of the fitted portion of the far-IR spectrum. Finally, the comparative success of this application of Mori theory indicates that an analytic model may be useful for extracting information contained in low-frequency spectra.

A value for K_2 , the value of the intermolecular torque correlation function at $t = 0$, obtained through molecular dynamics simulations should provide more physically grounded parameters for use in eq 10.^{16,41} An approach, which differs from Mori analysis mainly in the assumption that the torque correlation function is Gaussian, has been used with some success in describing effects of dielectric friction by Hochstrasser and co-workers.⁴² Applying MD simulations to this series of mixtures as well as the method of instantaneous normal modes is a future extension of this study on liquid mixtures.

Note Added in Proof: A preliminary account of this work has been presented elsewhere.⁴⁶

Acknowledgment. We thank Professor Dan Kivelson for discussion corroborating the shortcomings of the Mori formalism described herein. We acknowledge the National Science Foundation for partial financial support through Grants CHE-9357424 (B.N.F. and N.F.S.) and PHY-9422952 (R.A.C. and D.G.). N.F.S. is the recipient of a David and Lucille Packard Foundation Fellowship and is an Arnold and Mabel Beckman Young Investigator.

Appendix A

Absorption Coefficient from Experimental Data. A pair of measurements are required for a complete data set: the terahertz transmission spectrum through the empty cell and the terahertz spectrum through the cell plus liquid sample. The absorption coefficient was measured in a way similar to that of Katzenellenbogen et al.³³ Once the time domain data sets are prepared, as described in the Experimental Section, they are fast Fourier transformed such that

$$E(\omega) = E_0 e^{-i\omega t} e^{ikz} \quad (\text{A1})$$

where z is the path length and k is the frequency-dependent wave vector $k(\omega) = k' + ik''$. The power absorption coefficient, identical with twice the imaginary part of the wavevector, is obtained by deconvoluting the frequency domain data of the sample with that of the empty cell. The complex deconvoluted waveform may be expressed as

$$\frac{E_{\text{samp}}(\omega)}{E_{\text{ref}}(\omega)} = e^{-k''z} e^{i(k'-k_0)z} \quad (\text{A2})$$

where k_0 is the wave vector for radiation propagating in a vacuum. Hence, the frequency-dependent absorption coefficient $\alpha(\omega)$ is obtained from the absolute value of eq A2 as

$$\alpha(\omega) = -\frac{2}{l} \ln \left| \frac{E_{\text{samp}}(\omega)}{E_{\text{ref}}(\omega)} \right| \quad (\text{A3})$$

where l replaces z as the path length of the cell. The factor of 2 in eq A3 normalizes the imaginary part of the electric field in eq A2 to that of the intensity, the conjugate square of eq A2, by which the absorption coefficient is defined. The magnitude spectra and frequency-dependent absorption coefficients for all the solutions are shown in parts b and c of Figure 3.

Appendix B

PDA and CIA Components. The frequency-dependent absorption coefficient for comparison with experimental data for each of a series of mixtures of chloroform in carbon tetrachloride was calculated from the experimental data for the pure liquids. This function is

$$\alpha_{\text{mix}} = x_{\text{CHCl}_3} \alpha_{\text{CHCl}_3} + (1 - x_{\text{CHCl}_3})^2 \alpha_{\text{CCl}_4} \quad (\text{B1})$$

where x_{CHCl_3} denotes the mole fraction of CHCl₃, α_{CHCl_3} denotes the absorption coefficient of CHCl₃, and likewise for CCl₄. The quadratic factor before α_{CCl_4} occurs because collisionally induced absorption (CIA) arises through the interaction between two (or more) molecules. This model is simplistic in that the mole fraction weighted sum improperly weighs CIA between CHCl₃ molecules and ignores CIA between CHCl₃ and CCl₄ molecules. This expression includes all the discrimination between absorption components that the experimental data of the neat liquids allow.

Although a spectral fit for the mixtures that considers all types of absorption processes is not possible, the difference between CIA coefficients for CHCl₃ and CCl₄ may be calculated. A useful approximation (discussed below) will be to identify the absorption coefficient of neat chloroform (molecule type A) as being equal to the sum of the permanent dipolar absorption (PDA) and CIA contributions, that is,

$$\alpha_{\text{CHCl}_3} = \alpha_A + \alpha_{\text{AA}} \quad (\text{B2})$$

α_A denotes the absorption coefficient associated with the permanent dipole moment of CHCl₃, and α_{AA} denotes the coefficient for that absorption that is due solely to the transient dipole moment induced by collisions between two CHCl₃ molecules. The absorption coefficient for neat CCl₄ (molecule type B) is purely collisionally induced and may be written as

$$\alpha_{\text{CCl}_4} = \alpha_{\text{BB}} \quad (\text{B3})$$

Essentially, four mechanisms contribute to the absorption coefficient of the mixture: PDA of CHCl₃, CIA between CHCl₃ molecules, CIA between CCl₄ molecules, and CIA between

CHCl₃ and CCl₄ molecules. By use of the mole fractions of the mixtures to properly weight the four contributing absorption mechanisms, an expression for the absorption coefficient of the mixtures is obtained,⁴³

$$\alpha_{\text{mix}} = x_1 \alpha_A + x_1^2 \alpha_{\text{AA}} + (1 - x_1)^2 \alpha_{\text{BB}} + x_1(1 - x_1) \alpha_{\text{AB}} \quad (\text{B4})$$

where x_1 denotes the mole fraction of CHCl₃ in mixture 1, while α_A and α_{AA} are defined above. The product of mole fractions appears before each CIA term because CIA depends on the number of collisions. This number, say for the case of α_{AB} , increases in proportion to the number of each type of molecule present. This product of numbers of molecules is proportional to $x_1(1 - x_1)$ the product of mole fractions.⁴⁴ Substitution of eq B2 into eq B4 and identification of α_{BB} with the measured absorption coefficient for neat CCl₄ reduces eq B4 with one equation and three unknowns (α_A , α_{AA} , and α_{AB}) to one equation and two unknowns (α_{AA} and α_{AB}). Hence, the difference between the two unknown CIA coefficients is

$$\alpha_{\text{AB}} - \alpha_{\text{AA}} = \frac{\alpha_{\text{mix}} - x_1 \alpha_{\text{CHCl}_3} - (1 - x_1)^2 \alpha_{\text{CCl}_4}}{(x_1 - x_1^2)} \quad (\text{B5})$$

Substitution of eq B2 into eq B4 for α_A results in a small error in eq B5. That is, substitution of $\alpha_A = \alpha_{\text{CHCl}_3} - \alpha_{\text{AA}}$ into eq B4 results in the CIA term being weighted linearly when it should be weighted quadratically. This results in an overestimation of CIA between CHCl₃ molecules. This error is similar to that discussed in subsection D of Results and Discussion, where it was reasoned that linear weighting of a CIA term can be done with essentially negligible effect.

Integration of this difference over the frequency regime between 0 and 1.7 THz, the quietest region of the measured absorbance spectra, is performed by use of a Simpson's rule approximation over the first 28 points of the each absorption coefficient data set. As discussed in the text, the frequency-integrated difference in CIA contributions is 2.6 ± 0.4 THz cm^{-1} . The calculation of the frequency-integrated difference between CIA absorption coefficients was performed by applying Simpson's rule⁴⁵ to eq B5.

Appendix C

Generalized Langevin Equation. The principal goal of the Mori formalism is to re-express the primary variable (the molecular dipole moment in the current experiment) to consider the slow decay of the higher order derivatives of the primary variable. Correlations may persist for times comparable to the decay time of the time correlation function of the primary variable. The approach is based on the generalized Langevin equation, as the equation of motion for the evolution of the dipole moment vector, $\mathbf{f}_0(t)$, of a molecule in solution. The generalized Langevin equation description includes the vectors' normal motions, damping of the motion by the bath, and a description of the random fluctuations of the bath in the case where the random force correlation function is not a delta function (i.e., non-Markovian case). An outline of the Mori formalism²⁶ is presented in this section.

The dipole moment vector $\mathbf{f}_0(t)$ may be separated into components parallel and perpendicular to the direction of $\mathbf{f}_0(0)$,

$$\mathbf{f}_0(t) = P_0 \mathbf{f}_0(t) + (1 - P_0) \mathbf{f}_0(t) \quad (\text{C1})$$

where the operator P_0 projects the vector $\mathbf{f}_0(t)$ onto the $\mathbf{f}_0(0)$

axis and $(1 - P_0)$ projects $\mathbf{f}_0(t)$ onto an axis perpendicular to the $f_0(0)$ axis. Equation C1 may be rewritten as

$$\mathbf{f}_0(t) = \Xi_0(t)f_0 + f_0'(t) \quad (\text{C2})$$

where $f_0(0)$ has been denoted f_0 . (In the course of this derivation any variable that is not written explicitly as a function of time is meant to be the value of that variable at the zero of time.) The normalized dipole moment correlation function, $\Xi_0(t)$, is expressed as

$$\Xi_0(t) = \frac{\langle \mathbf{f}_0(t) f_0^* \rangle}{\langle f_0 f_0^* \rangle} \quad (\text{C3})$$

and the perpendicular projection term in eq C2 is

$$f_0'(t) = (1 - P_0)\mathbf{f}_0(t) \quad (\text{C4})$$

The precise expression of this component is critical for developing the time correlation functions of quantities closely related to the higher order derivatives of the primary variable, the ultimate goal of this application of the Mori formalism.

The Liouville equation of motion for $\mathbf{f}_0(t)$ is

$$\frac{d\mathbf{f}_0(t)}{dt} = iL\mathbf{f}_0(t) \quad (\text{C5})$$

Operating with $(1 - P_0)$ on eq C5 and substituting eq C2 for $\mathbf{f}_0(t)$ yields the differential equation

$$(1 - P_0) \frac{d}{dt} [\Xi_0(t)f_0 + f_0'(t)] = i(1 - P_0)L[\Xi_0(t)f_0 + f_0'(t)] \quad (\text{C6})$$

Simplification of eq C6 results through recognition that $P_0 f_0'(t) = 0$ and that $(1 - P_0)f_0 = f_0 - P_0 f_0 = 0$. The resulting equation of motion for $f_0'(t)$ is

$$\frac{df_0'(t)}{dt} = iL_1 f_0'(t) + \Xi_0(t)f_1 \quad (\text{C7})$$

where the identities

$$L_1 = (1 - P_0)L \quad (\text{C7a})$$

and

$$f_1 = iL_1 f_0 \quad (\text{C7b})$$

have been made and $f_1(0)$ is denoted f_1 . Equation C7, a first-order inhomogeneous differential equation, may be integrated by choosing a solution of the form $f_0'(t) = C(t) \exp(iL_1 t)$, solving for $C(t)$, substituting $f_0'(t) \exp(-iL_1 t)$ for $C(t)$, then solving for $f_0'(t)$. This procedure yields

$$f_0'(t) = \int_0^t \Xi_0(t)f_1(t-s) ds \quad (\text{C8})$$

where $f_1(t) = \exp(iL_1 t)f_1$. Substitution of eq C8 into eq C1 yields an expression that relates $\mathbf{f}_0(t)$ to $f_1(t)$.

$$\mathbf{f}_0(t) = \Xi_0(t)f_0 + \int_0^\infty \Xi_0(t)f_1(t-s) ds \quad (\text{C9})$$

Equation C9 illustrates a connection between the primary variable $\mathbf{f}_0(t)$ and $f_1(t)$, the component of the time derivative of $\mathbf{f}_0(t)$ perpendicular to $f_0(0)$ given by eq C7b. Inclusion of possibly non-negligible similarity in time correlation function

decay time between the primary variable and that of the time derivative of the primary variable is thereby achieved.

Solution of the Liouville equation for the general vector $f_j(t)$ is directly analogous to the above development for $\mathbf{f}_0(t)$. In the remaining derivation $f_j(0)$ is denoted f_j , similar to the shortened notation of f_0 and f_1 discussed above. This process may be summarized as follows:

1. use of the P_j and $(1 - P_j)$ operators to separate $f_j(t)$ into variables parallel and perpendicular to $f_j(0)$,
2. operation of $(1 - P_j)$ on and substitution of expression for f_j into the Liouville equation of motion for $f_j(t)$,
3. simplification of the Liouville equation to an equation of motion for $f_j'(t)$,
4. integration of the equation of motion to find the expression for $f_j'(t)$,
5. substitution of $f_j'(t)$ into the original expression for $f_j(t)$ to relate $f_j(t)$ to $f_{j+1}(t)$.

The expression analogous to eq C9 for the general vector $f_j(t)$ is²⁶

$$f_j(t) = \Xi_j(t)f_j + \int_0^t \Xi_j(s)f_{j+1}(t-s) ds \quad (\text{C10})$$

where, in analogy to eq C3,²⁶

$$\Xi_j(t) = \frac{\langle f_j(t) f_j^* \rangle}{\langle f_j f_j^* \rangle} \quad (\text{C11})$$

Differentiating eq C11 yields an equation of motion for $\Xi_j(t)$, but introduces a factor of $df_j(t)/dt$. Therefore, a relationship between $df_j(t)/dt$ and $f_j(t)$ needs to be established in order to benefit from having determined the connection between successive orders time derivatives of the primary variable. This relationship is simply obtained first by separating the right-hand side of the Liouville equation of motion for f_j into components parallel and perpendicular to the orientation of f_j at the zero of time. That is,

$$\frac{df_j}{dt} = P_j[iL_1 f_j] + i[(1 - P_j)L_j]f_j \quad (\text{C12})$$

Substitutions analogous to the identities made in eqs C7a and C7b and recognition that $iL_1 f_j = df_j/dt$ yields

$$\frac{df_j}{dt} = i\omega_j f_j + f_{j+1} \quad (\text{C13a})$$

where $i\omega_j$ is defined such that $i\omega_j f_j$ is the component of df_j/dt that is parallel to f_j . That is,

$$i\omega_j = \frac{\langle df_j/dt f_j^* \rangle}{\langle f_j f_j^* \rangle} \quad (\text{C13b})$$

Operation of the time propagation operator $\exp(iL_1 t)$ on eq C13a yields

$$\frac{df_j(t)}{dt} = i\omega_j f_j(t) + e^{iL_1 t} f_{j+1} \quad (\text{C14})$$

Substitution of eq C13a into the time derivative of eq C11 yields

$$\frac{d\Xi_j(t)}{dt} = i\omega_j \Xi_j(t) + \frac{\langle f_{j+1} f_j^*(-t)^* \rangle}{\langle f_j f_j^* \rangle} \quad (\text{C15})$$

Using $\Xi_j(s)^* = \Xi_j(-s)$ and substitution of eq C10 into eq C15

for f_{j+1} yields²⁶

$$\frac{d}{dt}\Xi_j(t) = \omega_j\Xi_j(t) - \int_0^t \Xi_{j+1}(t-s)\Delta_{j+1}^2\Xi_j(s) ds \quad (\text{C16})$$

where

$$\Delta_j^2 = \frac{\langle f_{jj}^* \rangle}{\langle f_{j-1j-1}^* \rangle} \quad (\text{C17})$$

Equation 1 in the Theory section follows directly from eq C16 in that eq 1 is the Laplace transformation eq C16.

References and Notes

- (1) Debye, P. *Polar Molecules*; Dover: New York, 1929.
- (2) Gordon, R. *J. Chem. Phys.* **1965**, *43*, 1307.
- (3) Xu, M.; Firman, P.; Petrucci, S.; Eyring, E. M. *J. Phys. Chem.* **1993**, *97*, 3968.
- (4) McQuarrie, D. *Statistical Mechanics*; Harper Collins: New York, 1976.
- (5) Maroncelli, M. *J. Chem. Phys.* **1991**, *94*, 2084.
- (6) Fleming, G. R.; Wolynes, P. *Phys. Today* **1990**, *May*, 36.
- (7) Kliner, D. A. V.; Alfano, J. C.; Barbara, P. F. *J. Chem. Phys.* **1993**, *98*, 5375.
- (8) Arnett, D. C.; Vöhringer, P.; Scherer, N. F. *J. Am. Chem. Soc.* **1995**, *117*, 12262.
- (9) Wynne, K.; Galli, C.; Hochstrasser, R. M. *J. Chem. Phys.* **1994**, *100*, 4797.
- (10) Ladanyi, B. M.; Stratt, R. M. *J. Phys. Chem.* **1996**, *100*, 1266.
- (11) Lian, T.; Kholodenko, Y.; Hochstrasser, R. M. *J. Phys. Chem.* **1995**, *99*, 2546.
- (12) Berne, B. *Correlation Functions*; Harper: New York, 1975.
- (13) Harde, H.; Katzenellenbogen, N.; Grischkowsky, D. *Phys. Rev. Lett.* **1995**, *74*, 1307.
- (14) Nee, T. W.; Zwanzig, R. *J. Chem. Phys.* **1970**, *52*, 6353.
- (15) Hubbard, J. B. *J. Chem. Phys.* **1978**, *69*, 1007.
- (16) Madden, P.; Kivelson, D. *Adv. Chem. Phys.* **1984**, *56*, 480.
- (17) Cross, A. J.; Simon, J. D. *J. Chem. Phys.* **1987**, *86*, 7079.
- (18) van der Zwan, G.; Hynes, J. T. *J. Phys. Chem.* **1985**, *89*, 4181.
- (19) Pedersen, J. E.; Keiding, S. R. *IEEE J. Quantum Electron.* **1992**, *28*, 2518.
- (20) Kindt, J. T.; Schmuttenmaer, C. A. *J. Phys. Chem.* **1996**, *100*, 10373.
- (21) Thrane, L.; Jacobsen, R. H.; Uhd Jepsen, P.; Keiding, S. R. *Chem. Phys. Lett.* **1995**, *240*, 330.
- (22) van Exter, M.; Fattinger, Ch.; Grischkowsky, D. *Opt. Lett.* **1989**, *14*, 1128.
- (23) Einstein, A. *Ann. Phys.* **1905**, *17*, 549.
- (24) Smoluchowski, M. v. *Ann. Phys.* **1906**, *21*, 756.
- (25) Langevin, P. *Compt. Rend.* **1908**, *146*, 530.
- (26) Mori, H. *Prog. Theor. Phys.* **1965**, *34*, 399.
- (27) Zwanzig, R. *J. Chem. Phys.* **1960**, *33*, 1338.
- (28) Gordon, R. G. *J. Chem. Phys.* **1963**, *38*, 1724.
- (29) Weast, R. C.; Lide, D. R. *CRC Handbook of Chemistry and Physics*; CRC Press: Boca Raton, FL, 1990.
- (30) Krausz, F.; Spielmann, Ch.; Brabec, T.; Wintner, E.; Schmidt, A. *J. Opt. Lett.* **1992**, *17*, 204.
- (31) Asaki, M. T.; Huang, C. P.; Garvey, D.; Zhou, J.; Kapteyn, H. C.; Murnane, M. M. *Opt. Lett.* **1993**, *18*, 977.
- (32) Vöhringer, P.; Westervelt, R. A.; Yang, T. S.; Arnett, D. C.; Feldstein, M. J.; Scherer, N. F. *J. Raman Spectrosc.* **1995**, *26*, 535.
- (33) Marshall, A. G.; Verdun, F. R. *Fourier Transforms in NMR, Optical, and Mass Spectrometry*; Elsevier: New York, 1990.
- (34) Katzenellenbogen, N.; Grischkowsky, D. *Appl. Phys. Lett.* **1991**, *58*, 222.
- (35) Harde, H.; Katzenellenbogen, N.; Grischkowsky, D. *JOSA B* **1994**, *11*, 1018.
- (36) Goulan, J.; Rivail, J. L.; Flaming, J. W.; Chamberlain, J.; Chantry, G. W. *Chem. Phys. Lett.* **1973**, *18*, 211.
- (37) Chandra, R.; Xu, M.; Firman, P.; Eyring, E. M.; Petrucci, S. *J. Phys. Chem.* **1993**, *97*, 12127.
- (38) Flanders, B. N.; Moore, P.; Grischkowsky, D.; Scherer, N. F. Work in progress.
- (39) Hynes, J. T. *J. Phys. Chem.* **1987**.
- (40) Ascarelli, G. *Chem. Phys. Lett.* **1976**, *39*, 23.
- (41) Adelman, S. A. *J. Chem. Phys.* **1976**, *64*, 124.
- (42) Pereira, M. A. C. Q. Ph.D. Thesis, University of Pennsylvania, 1990; p 97.
- (43) Pardoe, G. W. F. *Trans. Faraday Soc.* **1970**, *66*, 2699.
- (44) Moelwyn-Hughes, E. A. *Physical Chemistry*; Pergamon: New York, 1957; p 51.
- (45) Fogiel, M. *Handbook of Mathematical, Scientific, and Engineering Formulas, Tables, Functions, Graphs, Transforms*; Research and Education Association: Piscataway, NJ, 1988.
- (46) Flanders, B. N.; Cheville, R. A.; Grischkowsky, D.; Scherer, N. F. *Ultrafast Phenomena X*; Barbara, P., Knox, W., Zinth, W., Fujimoto, J., Eds.; Springer Series in Chemical Physics; Springer-Verlag: Berlin, 1996, in press.

JP960953C